Thermal Stability and Electrical Characteristics of Tungsten Nitride Gates in Metal–Oxide–Semiconductor Devices

2008 Jpn. J. Appl. Phys. 47 872

(http://iopscience.iop.org/1347-4065/47/2R/872)

Japanese Journal of Applied Physics
Vol. 47, No. 2, 2008, pp. 872–878

Thermal Stability and Electrical Characteristics of Tungsten Nitride Gates in Metal–Oxide–Semiconductor Devices

Chih-Feng HUANG*, Bing-Yue TSUI, and Chih-Hsun LU

Department of Electronics Engineering and Institute of Electronics, National Chiao Tung University, ED630, No. 1001, Ta-Hsueh Road, Hsinchu 300, Taiwan, R.O.C.

(Received June 17, 2007; accepted October 29, 2007; published online February 15, 2008)

Tungsten nitride (WN_x) was investigated to be used as a metal gate of metal–oxide–semiconductor field effect transistors (MOSFETs). WN_x films with various N/W atomic ratios were deposited on SiO_2 and HfO_2 by reactive sputter deposition at different N_2/Ar ratio flows. Nitrogen concentration in WN_x films increases rapidly with the N_2/Ar gas ratio and tends to saturate. WN_x films with nitrogen atomic ratio higher than 44% have a main phase of WN, and the WN phase is stable up to 800 °C. The higher-order WN_x phase does not form even if the nitrogen concentration is as high as 61%. Many of the excess nitrogen atoms in WN_x films are desorbed at temperatures below 766 °C. The excess nitrogen in WN_x films can cause effective work function lowering. A weak Fermi-level pinning effect is observed on the HfO_2 film. In this case, WN_x is not suitable to be metal gate of bulk p-channel MOSFETs. Fully depleted silicon-on-insulator (FD SOI) devices require a work function of 0.2 eV from the midgap of the Si energy band. Therefore, a WN_x/HfO_2 gate stack can be applied to p-channel FD SOI devices. The good integrity of the WN_x/HfO_2 gate stack also suggests that WN_x is a promising gate material.
[DOI: 10.1143/JJAP.47.872]

KEYWORDS: metal gate, WN, work function, MOSFET

1. Introduction

Refractory metals and their nitrides have wide spread applications in various fields including microelectronics due to their excellent hardness, high melting point, and good chemical stability. Among refractory metals, tungsten has attracted considerable attention in modern very large scale integrated circuits (VLSI) because of its low resistivity, easy patterning, and compatibility to conventional complementary metal–oxide–semiconductor (CMOS) technology.[1,2] Tungsten plugs have been used to electrically connect the multilevel interconnects in mass production. Tungsten nitride has also emerged as a promising candidate for the Cu diffusion barrier.[3] Metal gates are expected to replace polycrystalline silicon (poly-Si) gates beyond the 45-nm technology node to continue device scaling. Tungsten and its nitride (WN_x) were again considered as possible materials of metal gates since metal gates have been studied to replace poly-Si gates in the late 1970s because of their low resistivity.[1,2] Tungsten with a midgap work function was considered as a single metal gate of fully depleted silicon-on-insulator (FD SOI) CMOS devices to provide a symmetric threshold voltage for both n- and p-channel devices.[1,4] WN_x has a higher work function and was suggested as the metal gate of p-channel bulk MOS field effect transistors (MOSFETs).[5,6] There have been numerous studies on the basic material properties of WN_x films, including the crystalline structure, effects of nitrogen composition, resistivity, patterning, residual stress, and thermal stability.[7–10] Moreover, there are also some reports on the electrical characteristics and reliability of MOS devices with tungsten nitride gates.[11–14] An obvious phenomenon of nitrogen desorption from tungsten nitride films was noticed. However, electrical effects of nitrogen desorption in previous studies were not thoroughly explored.

In this work, nitrogen-rich tungsten nitride films deposited by reactive sputtering were used as electrodes of MOS capacitors with SiO_2 and HfO_2/SiO_2 stack gate dielectrics. The thermal stability and electrical stability were investigated after prolonged (30 min) post metal annealing at 400–800 °C in N_2 ambient. The effective work function of WN_x gates on SiO_2 and HfO_2 was first studied in the context of incorporated nitrogen concentration and interface bonds between WN_x electrodes and gate dielectrics. The electrical characteristics of MOS capacitors with a pure tungsten gate were also presented as a reference.

2. Experiments

Simple MOS capacitors were used as the test devices. The starting material were 6-in., (100)-oriented, and boron-doped p-type silicon wafers with a resistivity of 15–25 Ω cm. After wafer cleaning, oxide layers with various thicknesses of 40, 70, and 100 nm were thermally grown in dry O_2 ambient. Some wafers were then deposited with a 5-nm-thick HfO_2 film in a reactively sputtered deposition system with an Ar/O_2 gas ratio of 24 : 3. During the deposition, the chamber pressure was 7.6 mTorr and the DC power was 100 W. Neither substrate bias nor substrate heating was intentionally applied. Because the bottom oxide was thick enough, further oxidation during HfO_2 deposition did not occur.[15] After the preparation of gate dielectrics with a SiO_2 single layer and a HfO_2/SiO_2 stack, all of the wafers were annealed in N_2 ambient at 900 °C for 30 s by a rapid thermal annealing (RTA) to reduce the density of oxide charges and to form a stable microstructure of HfO_2, that will not changed again during the post metal annealing. A lift-off process was used to define the metal gate electrodes. The WN_x films with various N/W atomic ratios were reactively sputtered at 4.5 mTorr in a DC sputtering system to a thickness of 60 nm. The N_2/Ar gas flow ratios used in this work were 0 : 20, 5 : 20, 10 : 20, and 20 : 20. During deposition, the DC bias was set to 25 W and neither substrate bias nor substrate heating was applied. After the lift-off process, wafers were diced and annealed at 400, 500, 600, 700, and 800 °C in a N_2 ambient furnace for 30 min. Finally, the aluminum film was deposited on the wafer back

*E-mail address: jeffhuang.ee90g@nctu.edu.tw

Table I. WN_x sample conditions.

	WN-0	WN-1	WN-2	WN-3
N_2/Ar flow ratio	0/20	5/20	10/20	20/20
N (at. %) (as-deposited)	0	44	56	61
Resistivity (Ω cm) (as-deposited)	94.09	1322	1735	2438
Main phase	W	WN	WN	WN

surface by thermal evaporation to establish good ohmic contact. Table I lists the sample conditions.

The atomic compositions of WN_x samples were identified by Rutherford backscattering spectroscopy (RBS). The RBS spectra were taken using a van de Graaff accelerator with 2 MeV α particles and calibrated with bulk samples of gold and silicon. A graphite substrate was used instead of a silicon substrate to avoid the weak nitrogen signal of the WN_x layer overlapped with the strong Si signal of the substrate. A 30-nm-thick SiO_2 layer was deposited in a plasma-enhanced chemical vapor deposition (PECVD) system on the graphite substrate before WN_x film deposition to provide surface conditions similar to those of real SiO_2/Si samples. The crystalline phase of WN_x films was examined by the X-ray diffraction (XRD) technique using a MAC Science MXP18 XRD system with Cu Kα radiation. Thermal desorption spectroscopy (TDS) was used to detect the nitrogen desorption, and the nitrogen depth profile in the WN_x films was examined by the Auger electron spectroscopy (AES) using a Physical Electronics Auger 670 PHI Xi system. After removing the WN_x films, chemical bonds at the surface of HfO_2 were analyzed by X-ray photoelectron spectroscopy (XPS). The XPS spectra with 0.8 eV experimental resolution were recorded in a Physical Electronics PHI 1600 system, using an Mg Kα source operating at 250 W and 15 KeV.

The capacitance–voltage (C–V) curves of capacitors were measured at 100 kHz using an Agilent 4284A precision impedance meter, and the flatband voltage (V_{fb}) was extracted from the C–V curves. The effective work function was extracted by the typical method of extrapolating V_{fb} at zero equivalent-oxide-thickness (EOT) from the V_{fb} versus EOT plot.[15] Constant-voltage stress application was performed using an Agilent 4156C semiconductor parameter analyzer.

3. Results and Discussion

3.1 *Physical properties of N-rich WN_x films*

The WN_x films were deposited by reactive sputtering with a mixture of Ar and N_2 gases, and the increase in N_2 gas flow rate formed high-N-ratio WN_x films. Figure 1 shows the N concentration and corresponding resistivity of the as-deposited WN_x films. The N concentrations analyzed by RBS are 0, 44, 56, and 61 at. % for WN-0, WN-1, WN-2, and WN-3, respectively. The N concentration increases rapidly and then tends to saturate. The corresponding resistivities are 94.09, 1322, 1735, and 2438 μΩ cm, respectively. The resisitivities of the WN_x films are much higher than that of W_2N (220 μΩ cm) and are considered to originate from a high-order WN_x phase.[7,10] The typical tungsten nitride

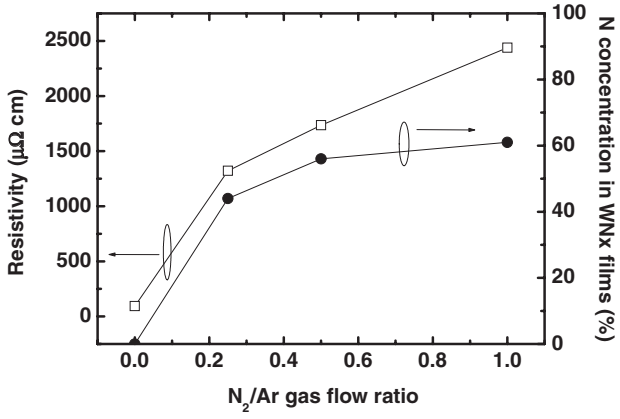

Fig. 1. Nitrogen concentration and relative resistivity of the WN_x films as a function of the N_2/Ar gas flow ratio during sputtering deposition.

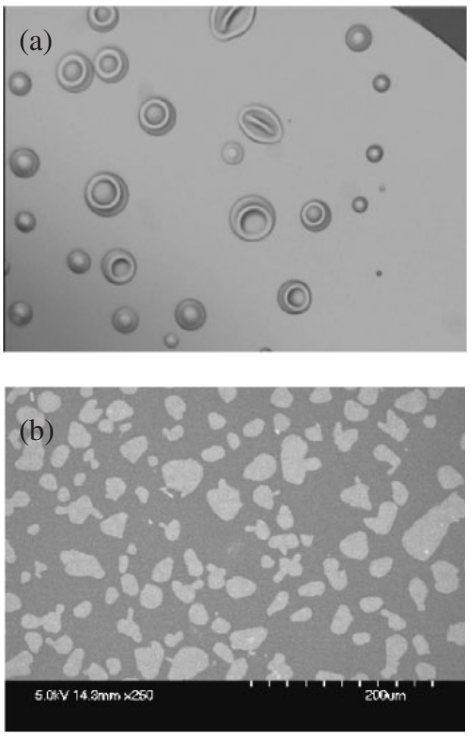

Fig. 2. Plane-view SEM micrographs of the WN-2 films after annealing at (a) 500 °C and (b) 800 °C in a rapid thermal annealing system. The temperature increase rate is 90 °C/s.

phases exist as W_2N or WN with 33.3 and 50% nitrogen stoichiometry, respectively. Because high-order WN_x phases are unstable, any further incorporation of N in WN_x films is difficult.[7,10] It is believed that the stability of the WN_x phase is dependent on its heat of formation. The heat of formation for W_2N is −5.3 kcal/mol and is slightly more exothermic than that for WN, −3.6 kcal/mol.[16] W_2N is the most stable tungsten nitride phase with a cubic crystal lattice.

To investigate the thermal properties of the N-rich WN_x films, high-temperature annealing was performed. After RTA at a temperature increase rate of 90 °C/s, the WN-2 and WN-3 films had bubbles or cracks. As shown in Fig. 2, the WN-2 film had bubbles at 500 °C and cracks at 800 °C. The phenomenon seems to involve gas expansion to create bubbles and bubble blowout to generate cracks in WN_x

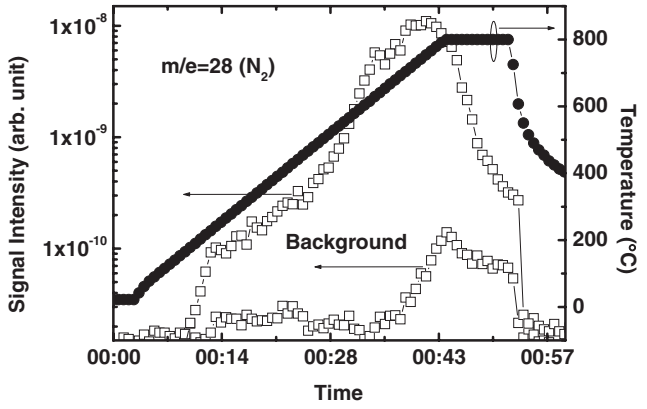

Fig. 3. Thermal desorption spectrum of the as-deposited WN-2 film.

films. TDS analysis was used to investigate the temperature-dependent thermal desorption of nitrogen. Figure 3 shows the background signal and sample signal of the WN-2/SiO_2 sample. The temperature increase rate was set at 20 °C/min. The intensity of the background signal is at least one order of magnitude lower than that of the sample signal and can be neglected. Nitrogen gas concentration increases rapidly with the temperature up to $T = 600$ °C and slowly reaches a maximum at $T = 766$ °C. After annealing at 800 °C for 10 min, the signal becomes weak. Most of the nitrogen not strongly bound with tungsten is desorbed at temperatures below 766 °C and the WN phase of WN-2 was identified by XRD. The sample after TDS analysis did not have bubbles and cracks. Therefore, the temperature increase rate of 20 °C/min during the TDS analysis was hence used for the furnace annealing to prevent film cracking.

The thermal desorption of nitrogen was detected by TDS analysis and then XPS analysis was used to detect if nitrogen diffuses into the under layer dielectric. After the tungsten nitride film was removed using H_2O_2 solution, the exposed surface of the dielectric was analyzed. The nitrogen distribution in the WN_x/SiO_2 structure has been analyzed by Yamada *et al.*[14] The nitrogen was incorporated at the interface between WN_x and SiO_2 during the reactive sputtering deposition of WN_x films and its concentration was the same after annealing for 30 min at 750 °C in N_2 ambient. The binding energy of N core level reflected major $N{\equiv}Si_3$ bonds and minor $Si{-}N{=}O_2$ bonds.[14] It was thus concluded that nitrogen does not diffuse into SiO_2 during annealing. In this work, we focus on the WN_x/HfO_2 structure. Figure 4 shows the core-level binding energies of O, Hf, and N for the 500 °C-annealed WN-1 sample. The binding energy of Hf core level only reflects Hf–O bonds. The signal of O binding energy is composed of two signals, one for N–O bonds and one for Hf–O bonds. The signal for the binding energy of N core level is very weak and represents N–O bonds. After 800 °C annealing, the binding energies of O and Hf are all the same as those of the 500 °C-annealed sample, and the area ratio of N–O and Hf–O is 1/4, which indicates that high-temperature annealing does not enhance the incorporation of N into the HfO_2 film.

The phases of the WN_x films were analyzed on the basis of the XRD patterns. Figure 5 shows the diffraction patterns of WN_x films annealed at different temperatures for 30

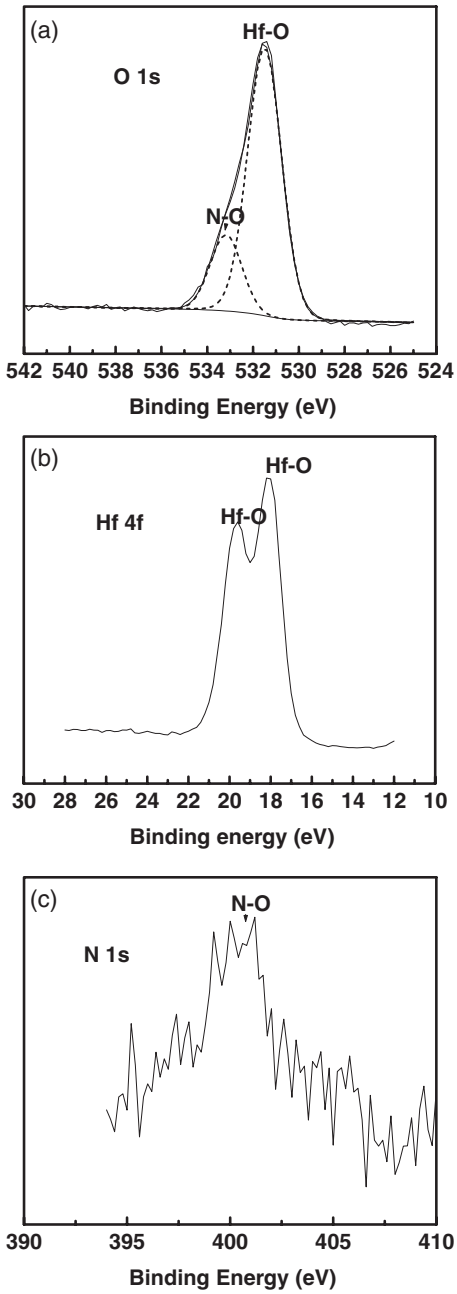

Fig. 4. XPS spectra of the (a) O 1s, (b) Hf 4f, and (c) N 1s of the WN-1 film after annealing at 500 °C for 30 min in N_2 ambient. The deconvolution of O 1s is also given.

min in N_2 ambient. The as-deposited WN_x films are all amorphous. After 600 °C annealing, the WN-1 film obviously reveals a WN phase. The WN-2 film is crystallized at 400 °C, and the main phase is still WN. The WN-3 sample is also crystallized at 400 °C and peak intensity increases with annealing temperature. The increase in nitrogen content to above 50% does not produce the higher-order WN_x phase, which confirms that the stable highest-order WN_x phase is WN after 800 °C annealing.[7,10] The broaden peak in WN-2 and WN-3 XRD spectra implies that the excess nitrogen can suppress grain growth. The relatively weak WO_3 phase is presumably due to the slight surface oxidation during annealing. The WN phase is stable up to 800 °C while it was reported that the WN and W_2N phases can change into the W phase at 900 °C in N_2 ambient, and the temperature for

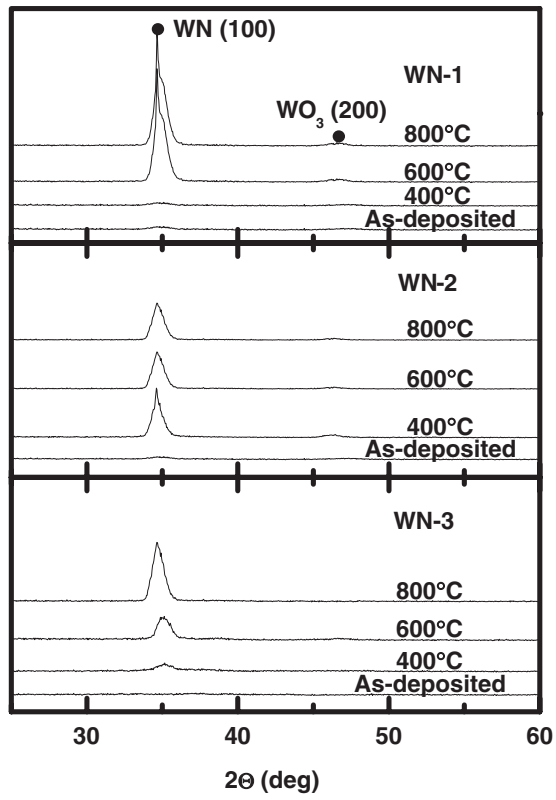

Fig. 5. XRD patterns of the WN_x films after annealing at different temperatures. All of the as-deposited films are amorphous.

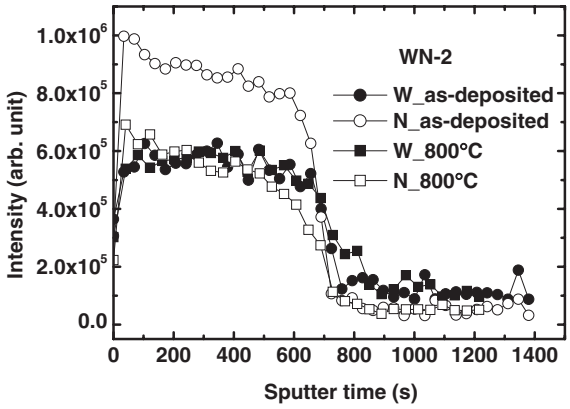

Fig. 6. AES depth profiles of the as-deposited and 800 °C-annealed WN-2 films.

phase transition is lower in H_2 and N_2 gas mixture ambient.[17] Since the phase of the annealed WN_x film is WN, unmerous N atoms in the as-deposited WN_x films are not strongly bounded to W. Figure 6 shows the nitrogen depth profile of WN-2 detected by AES. The intensity of the nitrogen signal for the 800 °C annealed WN-2/SiO_2 sample is much lower than that for the as-deposited sample, and the intensities of the W signal for both samples are the same. These physical analyses clearly confirm that nitrogen desorption occurred in the whole film after annealing.

3.2 *Electrical characteristic of MOS capacitor with WN_x gate*

The effective work function was extrapolated from the V_{fb}–EOT plot at zero EOT. For example, the V_{fb}–EOT plots

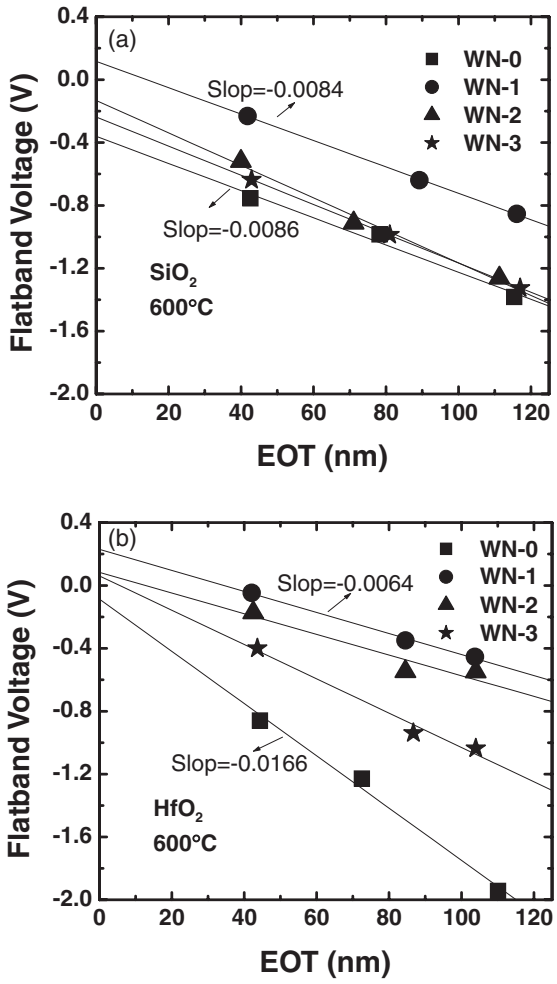

Fig. 7. V_{fb} vs EOT plots of (a) $WN_x/SiO_2/Si$ structure and (b) $WN_x/HfO_2/SiO_2/Si$ structure after annealing at 600 °C.

of 600 °C-annealed capacitors with SiO_2 and a HfO_2/SiO_2 stack are shown in Fig. 7. The good linearity reflects the validity of the effective work function extraction. For the single-layer SiO_2 samples, the y-axis intersection in the V_{fb}–EOT plot represents the work function difference between the metal gate and the Si substrate ($\Phi_{ms} = \Phi_m - \Phi_s$). It should be noted that the HfO_2 sample has a HfO_2/SiO_2 stack that affect the y-axis intersection point including the work function difference (Φ_{ms}) and the HfO_2/SiO_2 interface charges ($Q_{high\text{-}k/SiO_2}$). With the Si substrate concentration known, the effective work function of metal gate on SiO_2 can be extracted. However, on the HfO_2, an offset due to the $Q_{high\text{-}k/SiO_2}$ is inevitable. The evaluated work function of the HfO_2 sample will be denoted as $\Phi'_{m,eff}$ accounting for the offset. The detailed extraction procedure for effective work function has been discussed in literature.[15] The slopes of the SiO_2 curves are almost the same and reflect the positive oxide charges of about $1.8 \times 10^{11}\,cm^{-2}$ density. The slopes of HfO_2 curves indicate that the positive oxide charges decrease from 3.6×10^{11} to $1.5 \times 10^{11}\,cm^{-2}$. Compared with the pure W gate, all of the WN_x gates have few effective oxide charges. The reduction of the density of oxide charges is suspected to be due to the nitrogen plasma during reactive sputtering.

The effective work functions ($\Phi_{m,eff}$ and $\Phi'_{m,eff}$) of WN_x films on SiO_2 and HfO_2 after annealing are extracted and

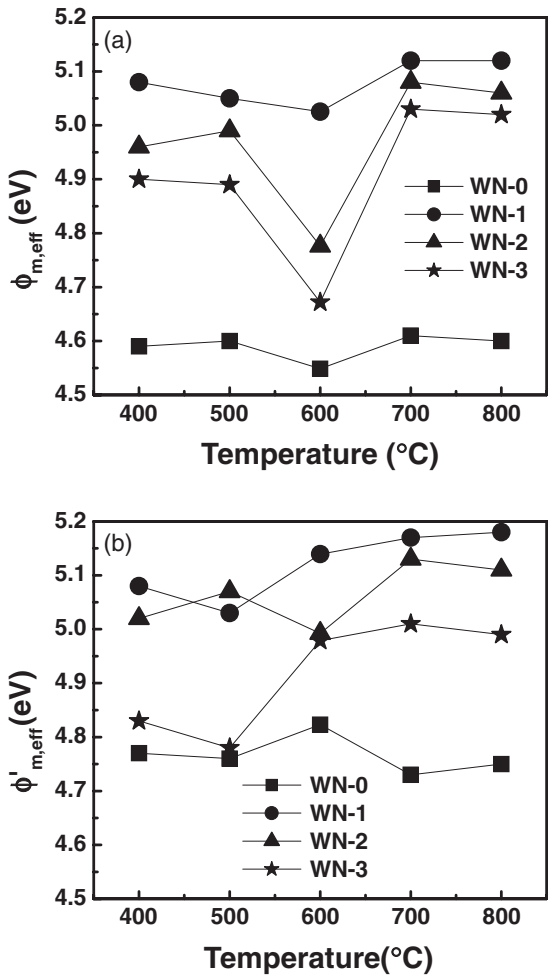

Fig. 8. Effective work functions ($\Phi_{m,eff}$ and $\Phi'_{m,eff}$) of WN_x on (a) SiO_2 and (b) HfO_2 as a function of annealing temperature. $\Phi'_{m,eff}$ takes into account the effect of interface charges between HfO_2 and SiO_2.

shown in Fig. 8. Regarding the WN_x on SiO_2, the $\Phi_{m,eff}$ of pure W (WN-0) is stable at ~4.60 eV below 800 °C, and the $\Phi_{m,eff}$ of tungsten nitrides seems to increase with annealing temperature and tends to approach a stable value at 700 °C. The WN-1, WN-2, and WN-3 samples annealed above 700 °C shows $\Phi_{m,eff}$ values of ~5.12, ~5.05, and ~5.0 eV, respectively. The effective work function of the metal gate is affected by its composition, orientation, phase, and interface interaction.[18,19] To explain the extracted work functions of WN_x films, these factors are considered. First, WN_x films do not chemically react with SiO_2 and HfO_2. Although the $N{\equiv}Si_3$ bonds and N–O bonds were observed at the interface between WN_x and the underlayer dielectric, these bonds are stable without further interaction below 800 °C.[14] The phase of the W film is W(110) below 900 °C.[10] The main phase of N-rich WN_x is WN(100) and stable up to 800 °C. Therefore, nitrogen incorporation in tungsten films forms the tungsten nitride compound (WN), which is the main reason why the effective work function changes from ~4.60 eV for the W phase to ~5.12 eV for the WN phase. The only parameter that changes during high-temperature annealing is the N content in WN_x. This suggests that the thermal instability of effective work function for WN_x comes from the excess nitrogen contents. This result is similar to that for MoN films.[20,21] The excess nitrogen atoms (piled-up nitrogen atoms) at the interface between MoN and SiO_2 reduce the $\Phi_{m,eff}$ value of MoN.[20,21] The nitrogen concentration at the interface determined the reduction of $\Phi_{m,eff}$.[20,21] Therefore, it is reasonable to conclude that WN-2 and WN-3 with more excess nitrogen have a relatively lower $\Phi_{m,eff}$ than WN-1. The WN_x films annealed at low temperatures have high contents of excess nitrogen to lower $\Phi_{m,eff}$. After high-temperature annealing ($T > 600$ °C), most of the excess nitrogen is desorbed so that $\Phi_{m,eff}$ reaches a high and stable value. Similarly, the results for WN_x/HfO_2 samples are determined by the nitrogen contents. The $\Phi'_{m,eff}$ values of pure W and WN-1 on HfO_2 are ~4.75 and ~5.18 eV after annealing at 800 °C, respectively.

The magnitude of work function adjustment ($\Delta\Phi'_{m,eff}$) on HfO_2 film is smaller than that on SiO_2 samples. This means that the WN_x deposited by reactive sputtering will cause the effective work function to be different if the dielectric is different. The difference may be affected by the work function offset due to interface charge ($Q_{high\text{-}k/SiO_2}$) between HfO_2 and SiO_2 and the Fermi-level pinning (FLP) effect.[22] Comparing pure W with WN-1 samples, the $\Delta\Phi'_{m,eff}$ values on HfO_2 ($\Delta\Phi_{m,eff}$ on SiO_2) films after annealing at 400 and 800 °C are 0.31 eV (0.50 eV) and 0.37 eV (0.52 eV), respectively. Moreover, comparing pure W with WN-3 samples, the $\Delta\Phi'_{m,eff}$ values on HfO_2 ($\Delta\Phi_{m,eff}$ on SiO_2) films after annealing at 400 and 800 °C are 0.05 eV (0.3 eV) and 0.21 eV (0.4 eV), respectively. The difference between $\Delta\Phi'_{m,eff}$ and $\Delta\Phi_{m,eff}$ increases slightly with nitrogen concentration. It is indeed necessary to consider if the interface dipole layer at the WN_x/HfO_2 interface induces the FLP effect. The reported FLP effects always force the work function of the metal gate to be pinned near the midgap of silicon.[22] Therefore, it is believed that FLP possibly occurs in the WN_x/HfO_2 stack. Because of the FLP effect, WN_x films are not suitable for bulk p-channel MOSFETs with a HfO_2 dielectric. The FLP effect shifts the work function to less than 0.15–0.2 eV, and WN_x can be sued in p-channel FD SOI devices.

Figures 9(a) and 9(b) show the statistic time-to-breakdown (T_{bd}) distributions of the WN_x/SiO_2 (5 nm)/Si and WN_x/HfO_2 (2 nm)/SiO_2 (2 nm)/Si MOS capacitors with different post metal annealing temperatures. The capacitance equivalent thickness (CET) of the HfO_2/SiO_2 stack is 3.5 nm. Samples were stressed at a constant voltage of $V_g = -6$ V for WN_x/SiO_2 capacitors and at $V_g = -4.5$ V for $WN_x/HfO_2/SiO_2$ capacitors because these samples have different gate dielectric thickness. Both are in the gate injection mode, and the electric field within the SiO_2 layer of HfO_2 and SiO_2 samples is ~12 MV/cm. It is found that the integrity of both SiO_2 and HfO_2/SiO_2 dielectrics with a pure W gate is not degraded during post metal annealing. On the other hand, the SiO_2 dielectric with a WN-1 gate is seriously degraded during the 700 °C post metal annealing while the HfO_2/SiO_2 dielectric with WN_x gates is not degraded. Compared with pure-W SiO_2 samples, the 500 °C and 600 °C WN-1 SiO_2 samples showed better time-dependent dielectric breakdown (TDDB) characteristics.

To better understand the TDDB characteristics, the current–voltage (I–V) curves shown in Fig. 10 were used to evaluate the effect of work function. The work functions of pure W is lower than that of WN-1, and the same bias

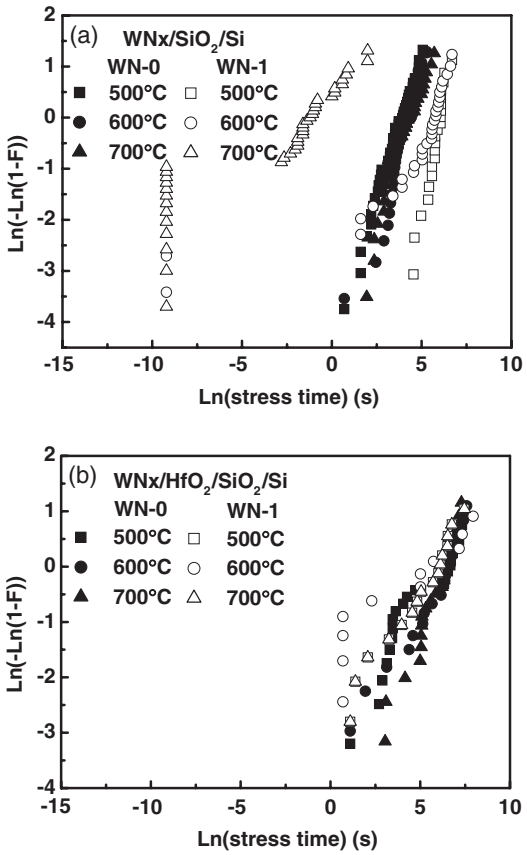

Fig. 9. Cumulative failure time of the (a) WN_x/SiO_2 (5 nm)/Si capacitors under constant-voltage stress at $V_g = -6$ V and (b) WN_x/HfO_2 (2 nm)/SiO_2 (2 nm)/Si capacitors under constant-voltage stress at $V_g = -4.5$ V as a function of annealing temperature.

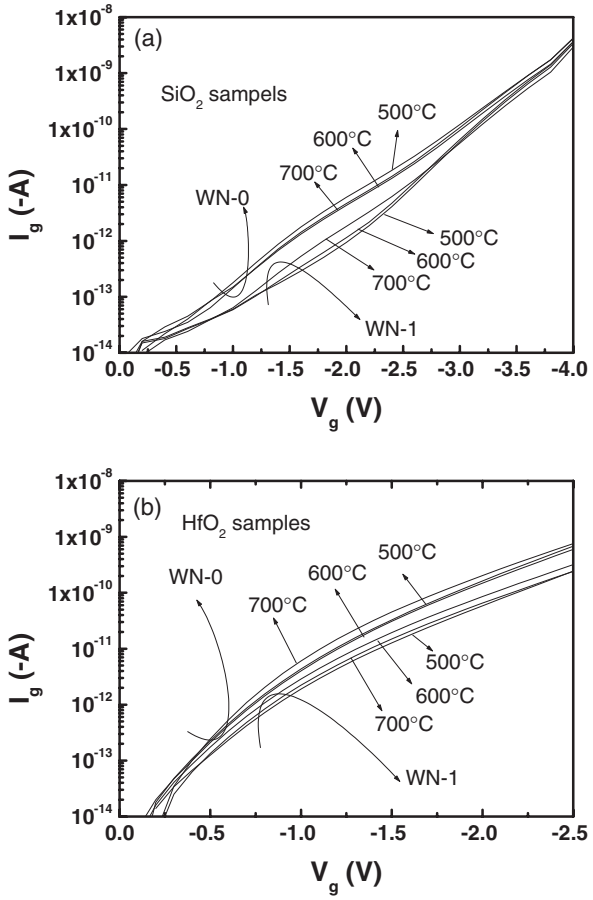

Fig. 10. *I–V* characteristics of (a) WN_x/SiO_2 (5 nm)/Si capacitor and (b) WN_x/HfO_2 (2 nm)/SiO_2 (2 nm)/Si capacitors.

stress will cause a relatively low leakage current for the WN-1 sample due to a high potential barrier for electrons on both SiO_2 and HfO_2 samples. This means that the stress condition at the same bias for the pure-W sample is stronger than that for the WN-1 sample, which is the reason why the SiO_2 samples with higher work functions have better TDDB characteristics.[23] The degradation of the 700 °C SiO_2 sample should be due to the creation of oxide defects, which is confirmed by the increased leakage current at low bias as shown in the *I–V* curves. Although the stress condition is stronger for the pure-W HfO_2 samples, the TDDB characteristics of pure-W samples are almost the same as those of WN-1 HfO_2 samples. It is reported that the time-to-breakdown (or charge-to-breakdown) for thin oxide (thickness less than 5 nm) is difficult to distinguish at high levels of electrical stress.[24] This is a possible reason why the TDDB characteristics are undistinguishable when comparing these pure-W samples with WN-1 HfO_2 samples. Moreover, the leakage current of the 700 °C annealed HfO_2 samples is not degraded. The degradation of the 700 °C-annealed WN-1/SiO_2 sample is suspected to be due to the stress exerted by the nitrogen desorption. Since the single SiO_2 layer cannot withstand post metal annealing, the HfO_2 layer of the HfO_2/SiO_2 stack acts as an effective buffer layer to prevent SiO_2 degradation from the WN_x gate during post metal annealing.

4. Conclusions

Tungsten nitride has an effective work function near the valance band of silicon so that it satisfies the metal-gate requirement of p-channel MOSFETs to provide a suitable threshold voltage. However, the excess nitrogen will make the work function unstable during high-temperature annealing, and may cause the WN_x film to crack during the high-temperature annealing with a high temperature increase rate. The post metal thermal annealing must be carefully controlled to avoid bubbling and cracking. The excess nitrogen in WN_x films can cause effective-work-function lowering. A weak Fermi-level pinning effect is observed on the HfO_2 film. In this case, WN_x is not suitable to be the metal gate of bulk p-channel MOSFETs. Fully depleted SOI devices require a work function lower than the Si valence band for p-channel MOSFETs and higher than the Si conduction band for n-channel MOSFETs. Therefore, the WN_x/HfO_2 gate stack can be applied to p-channel fully depleted SOI devices. The good integrity of the WN_x/HfO_2 gate stack also suggests that WN_x is as a promising gate material.

1) P. L. Shah: IEEE Trans. Electron Devices **26** (1979) 631.
2) A. K. Sinha, T. E. Smith, T. T. Sheng, and N. N. Axelrod: J. Vac. Sci. Technol. **10** (1973) 436.
3) B. H. Lee and K. Yong: J. Vac. Sci. Technol. B **22** (2004) 2375.
4) H. Noda, H. Sakiyama, Y. Goto, T. Kure, and S. Kimura: Jpn. J. Appl. Phys. **35** (1996) 807.
5) D.-G. Park, Z. J. Luo, N. Edleman, W. Zhu, P. Nguyen, K. Wong, C. Cabral, P. Jamison, B. H. Lee, A. Chou, M. Chudzik, J. Bruley, O. Gluschenkov, P. Ronsheim, A. Chakravarti, R. Mitchell, V. Ku,

H. Kim, E. Duch, P. Kozlowski, C. D. Emic, V. Narayanan, A. Steegen, R. Wise, R. Rengarajan, H. Ng, A. Sekiguchi, and C. H. Wann: Symp. VLSI Techology Tech. Dig., 2004, p. 186.
6) B. Claflin, M. Binger, and G. Lucovsky: J. Vac. Sci. Technol. A **16** (1998) 1757.
7) J. Lin, A. Tsukune, T. Suzuki, and M. Yamada: J. Vac. Sci. Technol. A **17** (1999) 936.
8) H.-T. Chiu and S.-H. Chuang: J. Mater. Res. **8** (1993) 1353.
9) Y. G. Shen and Y. W. Mai: J. Appl. Phys. **88** (2000) 1380.
10) C. C. Baker and S. Ismat Shah: J. Vac. Sci. Technol. A **20** (2002) 1699.
11) P.-C. Jiang and J. S. Chen: J. Electrochem. Soc. **151** (2004) G751.
12) H.-J. Cho, T.-H. Cha, K.-Y. Lim, D.-G. Park, J.-Y. Kim, J.-J. Kim, S. Heo, I.-S. Yeo, and J. W. Park: J. Electrochem. Soc. **149** (2002) G403.
13) J. W. Lee, C. H. Han, J.-S. Park, and J. W. Park: J. Electrochem. Soc. **148** (2001) G95.
14) T. Yamada, M. Moriwaki, Y. Harada, S. Fujii, and K. Eriguchi: Microelectron. Reliab. **41** (2001) 697.
15) B. Y. Tsui, C. F. Huang, and C. H. Lu: J. Electrochem. Soc. **153** (2006) G197.
16) J. W. Klaus, S. J. Ferro, and S. M. George: Appl. Surf. Sci. **162–163** (2000) 479.
17) Y. Z. Hu and S.-P. Tay: 10th IEEE Int. Conf. Advantage Thermal Processing of Semiconductors, 2002, p. 125.
18) K. Nakajima, Y. Akasaka, M. Kaneko, M. Tamaoki, Y. Yamada, T. Shimizu, Y. Ozawa, and K. Suguro: Symp. VLSI Technology Tech. Dig., 1999, p. 95
19) H. Wakabayashi, Y. Saito, K. Takeuchi, T. Mogami, and T. Kunio: IEDM Tech. Dig., 1999, p. 253.
20) P. Ranade, Y.-K. Choi, D. Ha, A. Agarwal, M. Ameen, and T.-J. King: IEDM Tech. Dig., 2002, p. 363.
21) P. Ranade, H. Takeuchi, T.-J. King, and C. Hu: Electrochem. Solid-State Lett. **4** (2001) G85.
22) Y.-C. Yeo, P. Ranade, T.-J. King, and C. Hu: IEEE Electron Device Lett. **23** (2002) 342.
23) D. J. DiMaria: J. Appl. Phys. **81** (1997) 3220.
24) I. C. Chen, S. Holland, and C. Hu: IEDM Tech. Dig., 1986, p. 660.